Coherence and stochastic resonance in a two-state system

Benjamin Lindner and Lutz Schimansky-Geier

Humboldt-University at Berlin, Invalidenstrasse 110, D-10115 Berlin, Germany

The subject of our study is a two-state dynamics driven by Gaussian white noise and a weak harmonic signal. The system resulting from a piecewise linear FizHugh-Nagumo model in the case of perfect time scale separation between fast and slow variables shows either bistable, excitable, or oscillatory behavior. Its output spectra as well as the spectral power amplification of the signal can be calculated for arbitrary noise strength and frequency, allowing characterization of the coherence resonance in the bistable and excitable regimes as well as quantification of nonadiabatic resonances with respect to the external signal in all regimes.

PACS number(s): 05.40.Ca

I. INTRODUCTION

Additive noise can have quite different effects when acting on oscillatory, excitable, or bistable dynamical systems. In the deterministic case an oscillatory system, e.g., a harmonic oscillator or limit cycle dynamics already possesses an eigenfrequency, which can be modified by random forcing [1]. In contrast to that, the influence of noise in excitable or bistable systems is more dramatic. Without any perturbation there is no response of the system at all, while too large fluctuations just result in a noisy output. In the case of an excitable system driven by an appropriate (moderate) amount of noise, however, the trajectory of the system can become quite regular, a phenomenon known as *autonomous stochastic resonance* [1,2] or *coherence resonance* (CR) [3–9]. It can either be understood as a noisy precursor of a bifurcation [4], e.g., a Hopf bifurcation, or be explained by means of the presence of different scaling behavior for the two time scales and their variance in excitable systems [3]. The trajectory in this case may be looked upon as the motion on a *stochastic limit cycle* [10,11] with a corresponding noise-induced eigenfrequency. For a given noise level, it might thus be impossible to distinguish between the excitable and the oscillatory system.

Bearing this in mind, we consider the response of both dynamics to additive weak periodic forcing. The oscillatory system driven by small fluctuations certainly displays a resonance with respect to the driving frequency. The same holds true for the excitable system in the case of a distinct eigenfrequency, i.e., in the case of CR. Since the considered systems are stochastic, this resonance results in a nonmonotonic dependence of the spectral power amplification (SPA) η as a function of driving frequency.

On the other hand, stochastic systems driven by a subthreshold signal can also exhibit *stochastic resonance* (SR) [12], i.e., the response of the system to a signal, e.g., the SPA, goes through a maximum as a function of *noise strength*. In particular, in excitable systems this has been verified for aperiodic driving (aperiodic SR) [13,14] and for harmonic driving [15–19]. In the latter case and from the point of view of SR the above supposed dependence of the SPA results in an additional improvement of SR by an appropriate tuning of the driving frequency. This has been shown by means of numerical simulations of an excitable

FitzHugh-Nagumo model driven by periodic force and noise [6]. A similar effect known as ''time scale matching'' was found by approximations and numerical studies of the leaky integrate-and-fire model [20–23] with periodic driving, which is a simple model for neuronal excitations.

In order to provide some insights into the interplay between the mentioned resonance effects in different dynamical regimes we consider in this study a simple two-state dynamics resulting from the limit case of a well-known stochastic system—the FitzHugh-Nagumo (FHN) model [24] driven by a weak harmonic signal and noise. The simplifications of the FHN model that we utilize are (a) a piecewise linear version of the widely used cubic null cline of the voltage variable, (b) a perfect time scale separation between fast and slow variables, and (c) a discretization of the voltage variable into two values representing the firing and the resting state, respectively. While (a) is rather a matter of taste because the FHN model itself is just a ''model of a model'' [25], the latter two assumptions actually imply neglect of subthreshold oscillations that are not relevant for the main excitation mechanism and its response to a weak signal if the voltage is considerably faster than the recovery variable. The resulting two-state dynamics may be regarded as a formal generalization of the model of a stochastic Schmitt trigger [26–28] but, in contrast to this device, displays not only bistable but also excitable or oscillatory behavior depending on system parameters and corresponding to various regimes of the FHN model. Using a method developed by Melnikov [28], spectral quantities of this system can be calculated analytically for *arbitrary* driving frequency and noise strength.

We start out with the reduction scheme for the FHN model yielding the two-state model. Then coherence resonance is quantified by means of the output spectrum in the absence of an external signal. Finally, we calculate the SPA in linear response theory [29] and discuss both resonances.

II. DERIVATION OF TWO-STATE DYNAMICS; FOKKER-PLANCK EQUATIONS

We consider the FHN model in a piecewise linear version [25]. With v being the fast voltage and u the slow recovery variable, this dynamics reads
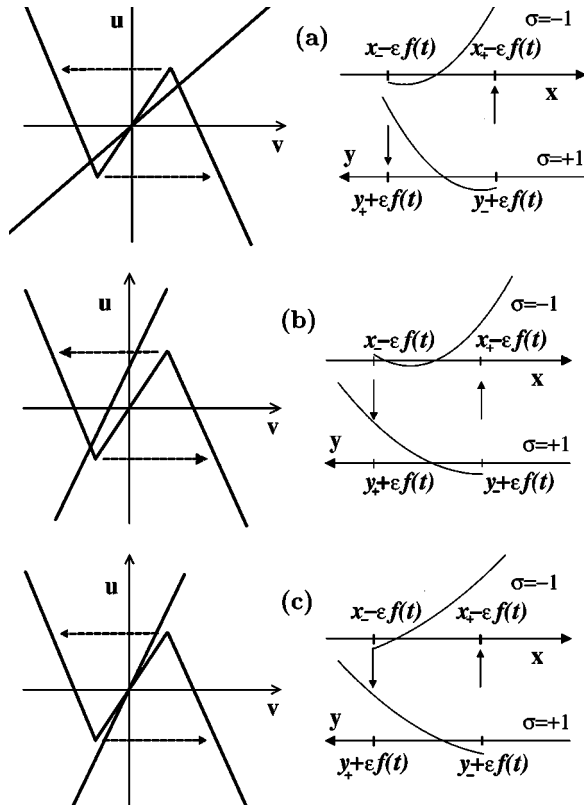
FIG. 1. Reduction of the two-dimensional dynamics to a two-state system. Possible transitions are indicated by arrows. (a) The bistable dynamics is mapped to a system with two stable states. (b) One stable fixed point (excitable regime) leads to one stable and one unstable state. (c) the limit cycle dynamics corresponds to a system without any stable state.

$$\tau \dot{v} = F(v) - u + c(t),$$

$$\dot{u} = \gamma v - u + b(t) + \sqrt{2Q}\xi(t), \qquad (1)$$

$$F(v) = \begin{cases} -1 - v, & v \leqslant -1/2 \\ v, & -1/2 < v < 1/2 \\ +1 - v, & v \geqslant 1/2. \end{cases}$$

Variables and parameters as well as all functions in the following are considered to be dimensionless. In Eqs. (1) $\xi(t)$ is Gaussian white noise, τ is the (small) time scale ratio of the two variables, and b, c are parameters (possibly time dependent, see below) determining the positions of the null clines $u = F(v) + c$ and $u = \gamma v + b$. Depending on the intersection points of these null clines (stable or unstable fixed points), we obtain either the bistable (two stable and one unstable fixed point), the excitable (one stable fixed point), or the oscillatory regime (one unstable fixed point) of the system (cf. Fig. 1, left side).

A weak signal $\tilde{f}(t) = \epsilon \cos(\Omega_s t)$ can enter the system (1) in different ways, additive in the equation of the recovery variable u [15–17] or in that of the voltage variable v [18,6], i.e., either

(I) $\quad b(t) = b_0 + \tilde{f}(t), \quad c = 0,$

$$\qquad (2)$$

or (II) $\quad b = b_0, \quad c(t) = \tilde{f}(t).$

By means of the simple transformation $\tilde{u} = u - c(t)$ Eqs. (1) can be recast into

$$\tau \dot{v} = F(v) - \tilde{u},$$

$$\qquad (3)$$

$$\dot{\tilde{u}} = \gamma v - \tilde{u} + b(t) - c(t) - \dot{c}(t) + \sqrt{2Q}\xi(t).$$

From these equations it becomes apparent that a difference between the two driving modes occurs for high frequencies only since in case (II) the effective amplitude of the signal scales with driving frequency Ω_s due to the temporal derivative, whereas in case (I) it does not.

The system we shall study is obtained for $\tau \rightarrow 0$, i.e., in the case of a perfect time scale separation of v and $\tilde{u}$. This limit is justified if one is not interested in subthreshold oscillations and other features occurring for a finite and not too small τ. It was recently shown [7] that for $\tau \rightarrow 0$ the two-dimensional dynamics (3) separates into two one-dimensional subsystems for the slow variable $\tilde{u}$. In other words, an adiabatic elimination of the fast variable v can be performed yielding a three-valued function $v(\tilde{u})$. Since the middle branch is unstable the relevant values are those corresponding to the left and right stable branches, i.e., to the mentioned subsystems. For these one-dimensional systems a linear force or a parabolic potential, respectively, is obtained due to (piecewise) linearity of the null clines. The points where the v null cline becomes unstable ($\pm 1/2, \pm 1/2$) are converted to absorbing boundaries (sink points), allowing transitions to the points with the same $\tilde{u}$ coordinate on the respective opposite branch (source points).

Introducing a new time scale $t \rightarrow t/(\gamma + 1)$ as well as new variables for the two subsystems

$$x = \tilde{u} - \frac{b_0 - \gamma}{1 + \gamma} - \epsilon f(t), \quad f(t) = A(\omega_s)e^{-i\omega_s t} + A^*(\omega_s)e^{i\omega_s t}$$

corresponding to the left branch and

$$y = -\tilde{u} + \frac{b_0 + \gamma}{1 + \gamma} + \epsilon f(t)$$

for the right branch leads to the dynamics

$$\dot{x} = -x + \sqrt{2D}\xi(t),$$

$$\qquad (4)$$

$$\dot{y} = -y + \sqrt{2D}\xi(t).$$

Here, a rescaled driving frequency $\omega_s = \Omega_s/(1 + \gamma)$ and noise strength $D = Q/(1 + \gamma)$ have been used. By our choice of variables the time dependent force is transformed to a modulation of the sink and source points, where the effective amplitude of the signal is modified by the prefactor

$$\text{(I)} \quad A_I = \frac{1/2}{(1+\gamma)(1-i\omega_s)},$$

$$\text{or (II)} \quad A_{II} = -\frac{1}{2}\frac{1/(1+\gamma)+i\omega_s}{(1-i\omega_s)}. \tag{5}$$

We note that for $\gamma \geq 0$ the absolute value of this prefactor is less than unity in both cases. The time dependent sink and source points of the system are given by

$$x_- - \epsilon f(t) = -\frac{1}{2} - \frac{b_0 - \gamma}{1+\gamma} - \epsilon f(t),$$

$$x_+ - \epsilon f(t) = \frac{1}{2} - \frac{b_0 - \gamma}{1+\gamma} - \epsilon f(t),$$

$$y_- + \epsilon f(t) = -\frac{1}{2} + \frac{b_0 + \gamma}{1+\gamma} + \epsilon f(t),$$

$$y_+ + \epsilon f(t) = \frac{1}{2} + \frac{b_0 + \gamma}{1+\gamma} + \epsilon f(t), \tag{6}$$

where x_-, y_-, x_+, y_+ are the (time independent) points of the unperturbed system ($\epsilon = 0$). In the subsequent sections we will consider the bistable and oscillatory case to be symmetric with respect to states ($x_- = y_-, x_+ = y_+$). Excitable systems are in this sense necessarily asymmetric. In particular, we choose

Regime	γ	b_0	$\rightarrow$	x_-	y_-	x_+	y_+
bistable	2/3	0	$\rightarrow$	-0.1	-0.1	0.9	0.9
excitable	1	2/5	$\rightarrow$	-0.2	0.2	0.8	1.2
oscillatory	7/3	0	$\rightarrow$	0.2	0.2	1.2	1.2

In the limit considered, the voltage variable $v(t)$ depends on $\tilde{u}$ and on the branch the system is currently occupying. The latter dependence carries the biophysically relevant information; it is thus justified to consider a discretized variable $\sigma(t)$ with two states $\sigma = \pm 1$ for the excited (right branch) and resting state (left branch), respectively, instead of the variable $v(t)$ itself. In the following we study the dynamics of this variable $\sigma(t)$ and its spectral properties.

Without signal ($\epsilon = 0$) the dynamics can be regarded as the motion of a Brownian particle jumping between two parabolic potentials. This is realized by absorption at the boundaries x_- or y_- (sink points) and by resetting to y_+ or x_+, the source points in the respective opposite state. The particle thus follows a circular flow $x_+ \rightarrow x_-$ jumping to $y_+ \rightarrow y_-$ and jumping back to x_+ (cf. Fig. 1) and generates the aforementioned two-state trajectory $\sigma(t)$. A state, e.g., the state $\sigma = -1$ corresponding to variable x, is left by relaxation from source to sink point if no potential minimum is present in this state, i.e., if $x_- > 0$. Then the state $\sigma = -1$ is unstable and in case of vanishing noise strength is left in a deterministic time. If there is a minimum, i.e., if $x_- < 0$, the

particle can escape from this stable state $\sigma = -1$ only by the action of noise due to the finite potential barrier at the sink point.

In principle, there are three different possibilities corresponding in a natural way to the three different regimes of the FHN model (see also Fig. 1): (a) two stable states (bistable regime), (b) one stable and one unstable state (excitable regime), and (c) two unstable states (oscillatory regime).

Case (a) coincides for $\gamma = b_0 = 0$, i.e., $x_+ = y_+ = -x_- = -y_-$, with a bistable symmetric Schmitt trigger (ST) driven by exponentially correlated noise and harmonic signal, which has been treated by Melnikov [28]. The formulas we shall present here are valid for the asymmetric Schmitt trigger as well [30], when $x_- = y_- + 2\delta$ and $x_+ = y_+ + 2\delta$ with δ as an asymmetry parameter. The reduction of the FHN model, however, results in a more general bistable behavior than this case. Consider, e.g., Fig. 1(a) where for an appropriate noise level a situation is realized for which relaxation into the potential minimum in *both* states takes a fairly long time compared to the escape time over the relatively small potential barrier at x_- and y_-. Clearly, this possibility is a consequence of the fact that the FHN model is a nonpotential system. For case (b) we note that the unstable state in the excitable case may be interpreted as the firing state of the system, whereas the ''nonfiring'' stable state represents both recovery (relaxation into the minimum) and resting state (position close to the minimum). In both cases (a) and (b), a finite noise strength is required in order to obtain a nonzero current in the system. This does not hold true in case (c)—with two unstable states the system works even without noise and switches periodically between $\sigma = +1$ and $\sigma = -1$ and back with $T_x = \ln(x_+/x_-)$ and $T_y = \ln(y_+/y_-)$, respectively.

With signal, the boundaries are modulated in time so that transitions are enhanced in one and suppressed in the other state for a given time. In this work, a signal is referred to as weak if it does not alter the currents of the system much; consequently, it should be subthreshold in cases (a) and (b). This definition also applies to case (c) where the system reaches the thresholds even in the absence of a signal.

Note that the system works like two coupled leaky integrate-and-fire (IF) models driven by external signal and noise where the absorption in one IF model is followed by reset to the other, and vice versa. A single IF model has recently been studied by different research groups [20–23]. In contrast to the common IF model, here the firing state is taken into account as a second state, allowing a well-defined approximation of the different regimes of the FHN model. Moreover, the reduction of the FHN model yields a linear dynamics of the slow variable in each state, whereas by the IF model the fast voltage variable is modeled. We would like to point out that Melnikov's method of calculating the spectrum and the SPA applies to the IF model too, without assuming an unphysiological reset of the signal phase after an absorption event as in [20,22].

The corresponding Fokker-Planck equations for Eq. (4) are given by

$$\partial_t P_x(x,t) = \partial_x(x + D\partial_x)P_x(x,t),$$

$$\partial_t P_y(y,t) = \partial_y(y + D\partial_y)P_y(y,t). \tag{7}$$

The densities P_x, P_y obey certain boundary and jump conditions. The probabilities vanish at the sink points,

$$P_x(x,t)|_{x_- - \epsilon f(t)} \equiv 0, \quad P_y(y,t)|_{y_- + \epsilon f(t)} \equiv 0. \quad (8)$$

Furthermore, continuity at the source points is required:

$$[P_x(x,t)]_{x_+ - \epsilon f(t)} \equiv 0, \quad [P_y(y,t)]_{y_+ + \epsilon f(t)} \equiv 0, \quad (9)$$

where the brackets denote the jump of a function $g(x)$: $[g]_x = g(x+0) - g(x-0)$.

Equations (7) are actually coupled by the condition that the probability efflux out of one state equals the influx into the other state, yielding

$$[\partial_x P_x(x,t)]_{x_+ - \epsilon f(t)} = -\partial_y P_y(y,t)|_{y_- + \epsilon f(t)}, \quad (10)$$

$$[\partial_y P_y(y,t)]_{y_+ + \epsilon f(t)} = -\partial_x P_x(x,t)|_{x_- - \epsilon f(t)}. $$

The total probability of both states is conserved and normalized to 1:

$$\int_{x_- - \epsilon f(t)}^{\infty} dx \, P_x(x,t) + \int_{y_- + \epsilon f(t)}^{\infty} dy \, P_y(y,t) = 1. \quad (11)$$

The process $\sigma(t)$ is entirely determined by these equations. The problem of computing its output spectrum in the absence and the SPA in the presence of a signal can be solved in a similar way as in [28]. Therefore, we shall just give the main results and refer the interested reader to [28] for details.

III. SYSTEM WITHOUT SIGNAL: COHERENCE RESONANCE

If no signal is applied to the system ($\epsilon = 0$) the stationary solution of Eq. (7) can readily be calculated. Normalization of this solution yields the stationary current

$$J_0 = \left(\int_{x_-/\sqrt{2D}}^{x_+/\sqrt{2D}} dz \, e^{z^2} \mathrm{erfc}(z) + \int_{y_-/\sqrt{2D}}^{y_+/\sqrt{2D}} dz \, e^{z^2} \mathrm{erfc}(z) \right)^{-1} / \sqrt{\pi}. \quad (12)$$

which on the one hand is identical with the stationary excitation rate (pulse rate) of the system and on the other hand coincides with the inverse of the sum of the mean first passage times $x_+ \to x_-$ and $y_+ \to y_-$. The time scale given by this rate can be expressed by a frequency

$$\omega_m = 2\pi J_0. \quad (13)$$

The output power spectrum for the process $\sigma(t)$ is given by the characteristic functions [31], i.e., the Fourier transforms $w_x(\omega), w_y(\omega)$ of the waiting time distributions of the states $\sigma = -1$ and $\sigma = +1$:
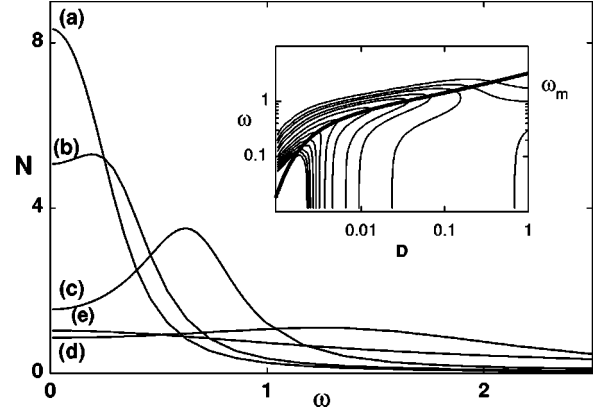

FIG. 2. Output spectrum of the bistable system (without signal) versus frequency for different noise levels (a)–(e): $D = 0.0024, 0.0031, 0.0089, 0.1226, 1.0$. Inset: Contour plot of spectral density versus D and ω compared with the mean frequency $\omega_m(D)$ (thick line) from Eq. (13).

$$N(\omega) = \int_{-\infty}^{\infty} d\tau \langle \sigma(t)\sigma(t+\tau) \rangle e^{i\omega\tau}$$

$$= \frac{8J_0}{\omega^2} \mathrm{Re} \left(\frac{[1 - w_x(\omega)][1 - w_y(\omega)]}{1 - w_x(\omega)w_y(\omega)} \right). \quad (14)$$

These waiting time distributions can be calculated by Laplace transformation of Eq. (7) and appropriate initial conditions as in [28], yielding

$$w_x(\omega) = \frac{\Psi_{x_+}(\omega)}{\Psi_{x_-}(\omega)} = \frac{e^{(x_+^2 - x_-^2)/4D} U(-i\omega - \frac{1}{2}, x_+/\sqrt{D})}{U\left(-i\omega - \frac{1}{2}, x_-/\sqrt{D}\right)}, \quad (15)$$

$$w_y(\omega) = \frac{\Psi_{y_+}(\omega)}{\Psi_{y_-}(\omega)} = \frac{e^{(y_+^2 - y_-^2)/4D} U(-i\omega - \frac{1}{2}, y_+/\sqrt{D})}{U\left(-i\omega - \frac{1}{2}, y_-/\sqrt{D}\right)},$$

where the numerators and denominators define $\Psi_{z_\pm}$ and $U(a,z)$ denote the parabolic cylinder functions [32].

The spectrum thus reads

$$N(\omega)$$

$$= \frac{8J_0}{\omega^2} \mathrm{Re} \left(\frac{[\Psi_{x_-}(\omega) - \Psi_{x_+}(\omega)][\Psi_{y_-}(\omega) - \Psi_{y_+}(\omega)]}{\Psi_{x_-}(\omega)\Psi_{y_-}(\omega) - \Psi_{x_+}(\omega)\Psi_{y_+}(\omega)} \right). \quad (16)$$

For the bistable case of a symmetric Schmitt trigger ($x_+ = y_+ = -x_- = -y_-$) treated by Melnikov this spectrum exhibits a Lorentz-like shape for arbitrary noise strength. There is no maximum at a finite frequency. In contrast, for the above mentioned bistable case of long lasting relaxation at small barriers for both states, i.e., $x_+ > |x_-|$ and $y_+ > |y_-|$, the output spectrum displays for an intermediate noise strength a peak at finite frequency (Fig. 2), indicating a regu-
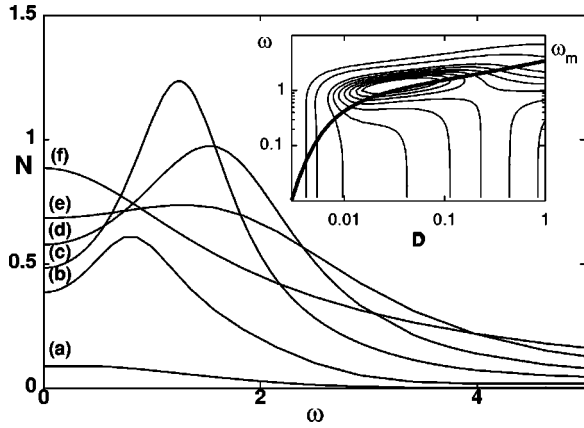
FIG. 3. Output spectrum of the excitable system (without signal) versus frequency and different noise levels (a)–(f): $D = 0.004, 0.009, 0.033, 0.094, 0.207, 0.769$. Inset: Contour plot of spectral density versus D and ω compared with the mean frequency $\omega_m(D)$ (thick line) from Eq. (13).

FIG. 4. Output spectrum of the oscillatory system (without signal) versus frequency for different noise levels (a)–(e): $D = 0.0018, 0.006\,84, 0.0195, 0.0558, 0.35$. Inset: Contour plot of spectral density versus D and ω compared with the mean frequency $\omega_m(D)$ (thick line) from Eq. (13).

lar behavior. This is an example of coherence resonance in a bistable system caused by large quasideterministic times of relaxation in both states. Consequently, it is a result of the nonpotential character of the FHN model. The noise-induced eigenfrequency, i.e., the position of the peak, nearly coincides with the mean frequency of the system given by Eq. (13) (cf. the contour plot in Fig. 2). Of course, the height and width of the observed peak can be improved by decreasing the distances of the minima to the sink points $|x_-|$ and $|y_-|$.

The spectrum of the excitable system for $x_- < 0$, $y_- > 0$ is depicted in Fig. 3. It starts at small noise intensity at a low level for all frequencies. The intensity of the process vanishes for decreasing noise in contrast to the same limit in the bistable regime. For increasing noise a peak appears, shifting first to larger and then back to lower frequencies, where it vanishes for large noise intensity. The peak height as a function of D goes through a maximum which is again a manifestation of coherence resonance. Clearly, the effect is more pronounced than in a comparable bistable system (e.g., for $y_- \to -|y_-|$) due to the presence of only one barrier in the system. Comparison of the contour lines of the spectral density with the mean frequency ω_m from Eq. (13) shows that—within the relevant parameter range—the induced eigenfrequency is larger than the mean frequency. If the system is ''more easily excitable,'' i.e., if $x_- \to 0$ relevant contributions to higher harmonics are also obtained, and the spectrum looks very similar to that of the oscillatory system for small noise.

The spectrum for the symmetric oscillatory case ($x_- = y_- > 0$, $y_+ = x_+$) is shown in Fig. 4 as a function of frequency and for different noise strength. Note that the spectral density is scaled logarithmically. For low noise intensity we obtain high peaks close to the (deterministic) fundamental
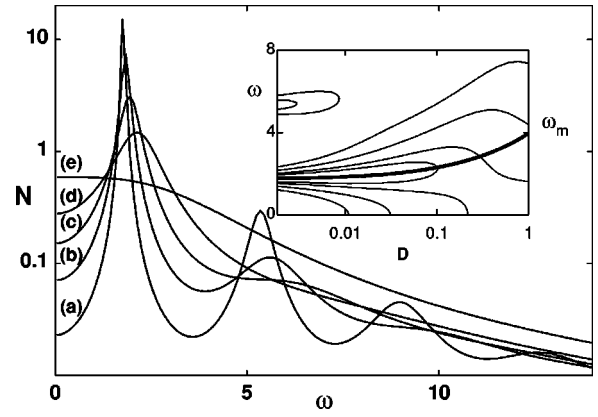
frequency $\omega_0 = \pi / \ln(x_+ / x_-)$ and its (odd) harmonics. The mean frequency (cf. the contour plot in Fig. 4) does not vanish for $D \to 0$ as in bistable or excitable systems but tends to ω_0. With growing noise the peaks are shifted toward higher frequencies, an effect that was found numerically in [1], and then peaks at higher harmonics vanish. Finally, the peak close to the fundamental frequency also disappears and a Lorentz-like shape of the spectrum is observed for large noise strength.

IV. SYSTEM WITH SIGNAL: STOCHASTIC RESONANCE

The amplification of a small signal $\epsilon f(t) = \epsilon(A e^{-i\omega_s t} + \text{c.c.})$ can be calculated in linear response using the asymptotic solutions $P_x(x,t)$, $P_y(y,t)$ for which the following ansatz is made:

$$P_x(x,t) = P_x^0(x) + \epsilon \exp\left(\frac{x_+^2 - x^2}{4D}\right)[A e^{-i\omega_s t} r_x(x) + \text{c.c.}],$$

and likewise for $P_y(y,t)$. Here, c.c. denotes the complex conjugate and $P_x^0(x)$ the stationary solution of Eq. (7). By inserting $P_x(x,t)$ and $P_y(y,t)$ into Eq. (7) the general solutions for $r_x(x)$ and $r_y(y)$ are found, again, in terms of parabolic cylinder functions. A linear expansion of the boundary and jump conditions in Eqs. (8–10) then fixes the free constants of these solutions. The current between the states, which can be calculated from these solutions, contains a time dependent part proportional to the external signal. This part leads to a δ function at the driving frequency with the amplitude $\epsilon^2 \eta$, where the SPA η after a lengthy calculation is obtained as

$$\eta(\omega_s, D) = \frac{8 J_0^2 |A|^2 \pi}{D} \left| \frac{(\Psi_{y_+} - \Psi_{y_-})(\Phi_{x_-} - \Phi_{x_+}) + (\Psi_{x_+} - \Psi_{x_-})(\Phi_{y_-} - \Phi_{y_+})}{\Psi_{x_-}\Psi_{y_-} - \Psi_{x_+}\Psi_{y_+}} \right|^2. \tag{17}$$
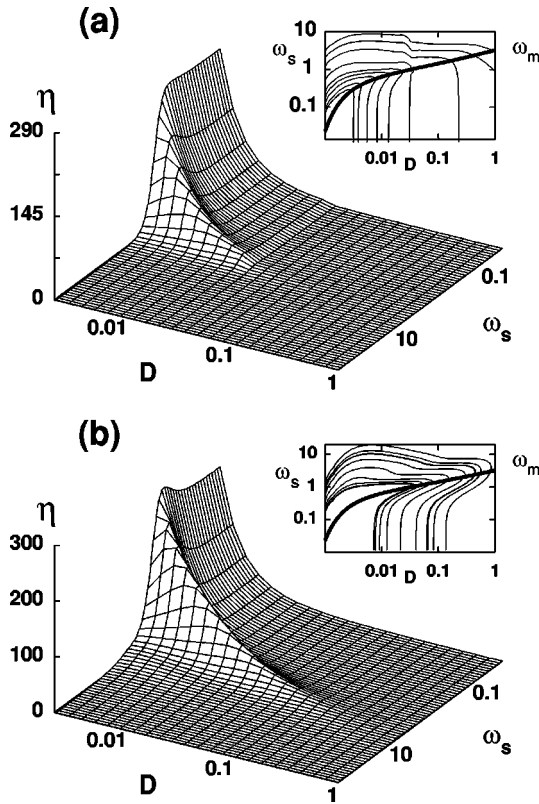
FIG. 5. Spectral power amplification versus frequency and noise level for the bistable system for the driving modes (I) (a) and (II) (b). Inset: Contour plot of spectral amplification versus D and ω_s compared with the mean frequency $\omega_m(D)$ (thick line) from Eq. (13).
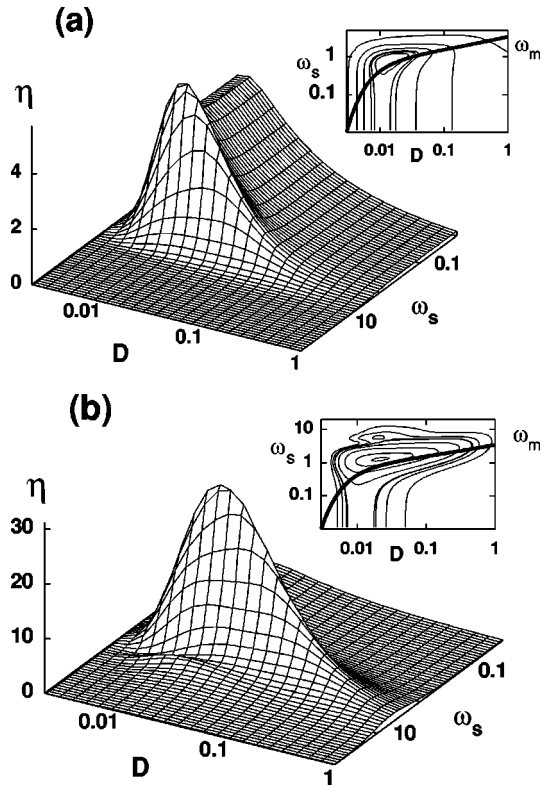

FIG. 6. Spectral power amplification of the excitable system versus driving frequency and noise strength for different driving modes (I) (a) and (II) (b). Note that two maxima occur at roughly the same noise intensity. Inset: Contour plot of spectral amplification versus D and ω_s compared with the mean frequency $\omega_m(D)$ (thick line) from Eq. (13).

The functions Φ_z in Eq. (17) differ from Ψ_z just by the first argument $-i\omega_s+1/2$. For the prefactor A either A_I or A_{II} (according to the driving mode under consideration) has to be inserted. Since $|A_{II}|^2$ and $|A_I|^2$ differ by the factor $[1+(1+\gamma)^2\omega_s^2]$, a larger value of the SPA is expected for harmonic driving of the fast variable [case (II)] than for that of the slow variable [case (I)]. It turns out that all observed effects of the SPA frequency dependence are much more pronounced in the former case. This is remarkable because a periodic signal in the equation for the voltage variable [case (II)] seems to be more justified from a neurobiological point of view.

We now consider the amplification as a function of noise strength and driving frequency for the regimes discussed in the preceding section for both driving modes.

For the bistable symmetric system we find a well-pronounced maximum with respect to D which manifests the occurrence of SR (Fig. 5). For any finite driving frequency the common stochastic resonance curve $\eta(D)$ displaying the well-known maximum is obtained (actually, this is shown for $w_s>0.45$ only). Additionally, a nonmonotonic dependence of the SPA on the driving frequency is observed. It is found for an intermediate range of noise intensities roughly corresponding to the range where coherence resonance in the bistable regime occurs. At a fixed noise level the system shows an optimal response to an external signal with frequency close to the noise-induced eigenfrequency of the system.

In Figs. 5(a) and 5(b) the mean frequency ω_m is again plotted as a function of D and compared to the contour lines, showing a time scale matching between ω_m and the optimal frequency for a large range of noise intensity and both driving modes. We once more point out that this effect is a consequence of the nonpotential character of the FHN model. It is not expected to occur in common bistable systems like the continuous overdamped bistable oscillator [12] or the symmetric Schmitt trigger [27]. Clearly, there is no overall maximum of the SPA η versus D and ω_s for $w_s>0$, exactly as in the bistable systems mentioned. A decrease of the driving frequency always yields an increasing maximum of η as a function of D.

In the excitable dynamics (Fig. 6) the resonance effect is much more pronounced; the SPA η shows a global maximum with respect to noise strength and driving frequency. At low frequencies the amplification reaches a limiting curve, as is known from asymmetric bistable systems [12]; the maximal SPA at moderate frequencies compared to this adiabatic limit is considerably larger in case (II) [note the different scale of η in Figs. 6(a) and 6(b)]. Similarly to the noise-induced frequency, the optimal driving frequency does not match the mean frequency ω_m of the system. However, all three frequencies differ just slightly and are of the same order of magnitude.

The occurrence of the global maximum can be considered in two different ways: (1) for fixed noise strength as a common resonance with respect to the noise-induced eigenfre-
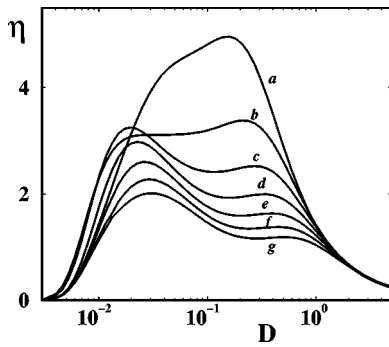
FIG. 7. Spectral power amplification in the excitable case and driving mode (II) versus noise intensity at different values of driving frequency (a)–(g): $\omega_s = 4,5,6,7,8,9,10$.

quency or (2) as a stochastic resonance which can be optimized by an appropriate tuning of the driving frequency. Another effect for the driving mode (II) is the occurrence of a second maximum with respect to driving frequency [Fig. 6(b)]. For frequencies beyond the frequency yielding the global maximum we find that the SPA as a function of D remains nearly constant over one order of magnitude of D (cf. Fig. 7). This is shown for driving mode (II) in Fig. 7. Note in particular curve b corresponding to $\omega_s = 5$. The amplification in this region can even display two maxima with respect to noise strength. Although the amplification in that parameter range is one order of magnitude smaller than the global maximum it is remarkable that the system is quite insensitive to the level of fluctuations. This is—apart from the well-known example in [33]—possibly another inherent mechanism of neuronal systems enabling them to detect weak signals without tuning noise intensity.

Finally, we turn to the spectral power amplification of the symmetric oscillatory case presented in Fig. 8. As for the spectral density, we find for a low noise level peaks at the basic deterministic frequency ω_0 and its higher odd harmonics. This is due to the fact that the ''spectrum'' of the deterministic system even without signal ($\epsilon = 0$) displays δ spikes at these frequencies; consequently the SPA η defined as the weight of the peak divided by the square of the signal amplitude ϵ^2 has to diverge in the limit $D \to 0$. More surprisingly, in this limit the amplification of a detuned signal [$\omega_s \neq (2m+1)\omega_0$] tends to finite values, as can be shown by a small D expansion of Eq. (17) (note that our system is averaged with respect to the initial phase of the signal).

Furthermore, if the driving frequency is between an odd and an even multiple of ω_0 the oscillatory system has possibly an optimal output at a finite noise level (cf. Fig. 9), although no potential barrier is present in the system. A similar effect has been found in a periodically modulated Wiener process [34]. Noise simply facilitates the detection of a ''positively detuned'' signal, since the eigenfrequency of the system increases with growing noise and thus for a certain noise level matches the signal frequency. This is, of course, limited by the fact that the entire system becomes more noisy, which destroys the cooperative effect; therefore the difference between the driving frequency and the natural frequencies of the system has to be smaller than the distance to the next (even) harmonics.
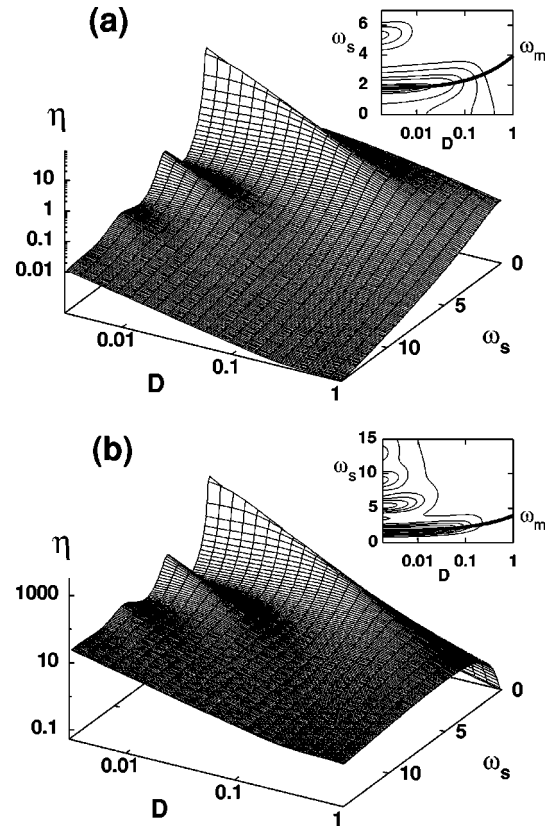

FIG. 8. Spectral power amplification of the oscillatory system versus frequency and noise level for different driving modes (I) (a) and (II) (b). Inset: Contour plot of spectral amplification versus D and ω_s compared with the mean frequency $\omega_m(D)$ (thick line) from Eq. (13).

A final remark concerns the signal-to-noise ratio (SNR) of the response. It can readily be calculated as the ratio of the amplification given by Eq. (17) and the spectrum at the driving frequency (14), serving as an approximation for the background noise at small signal amplitudes. However, this function does not show the relevant resonance of the system, for instance, in the excitable regime with respect to ω_s. The SNR in this case either increases to infinity for increasing frequency (second driving mode) or falls rapidly off (first driving mode). It is our belief that the system is rather characterized by the coherent part of the output, quantified by η,
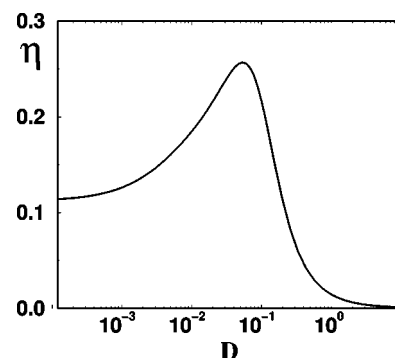

FIG. 9. Spectral power amplification for driving mode (I) in the oscillatory case versus noise intensity at $\omega_s = 3.0$ with the deterministic eigenfrequency $\omega_0 \approx 1.79$.

than by a ratio that is not ''noticed'' by a neuronal system and has been introduced in a more technical context [26].

V. CONCLUSIONS

We have presented results for a solvable two-state system that is the limit case of a stochastic FitzHugh-Nagumo model and possesses either bistable, excitable, or oscillatory behavior. Various nonadiabatic resonances of the system with and without two different kinds of periodic driving have been discussed. Coherence resonance, i.e., the occurrence of a noise-induced eigenfrequency, could be verified in the bistable and the excitable regime, resulting in a nonmonotonic dependence of the spectral amplification when a harmonic signal is added. This effect is much more pronounced if the signal is acting directly on the voltage variable of the FHN model. Furthermore, we have found that in the oscilla-

tory case an improvement of the signal detection with the assistance of noise is possible if the signal frequency is slightly larger than the deterministic eigenfrequency or than an odd harmonics of it. All results show selectivity of signal detection of weak *nonadiabatic* signals with respect to the driving frequency, and thus might be relevant for neurobiological applications of the model.

ACKNOWLEDGMENTS

[1] Hu Gang, T. Ditzinger, C. Z. Ning, and H. Haken, Phys. Rev. Lett. **71**, 807 (1993).

[2] A. Longtin, Phys. Rev. E **55**, 868 (1997).

[3] A. Pikovsky and J. Kurths, Phys. Rev. Lett. **78**, 775 (1997).

[4] A. Neiman, P. I. Saparin, and L. Stone, Phys. Rev. E **56**, 270 (1997).

[5] S. Lee, A. Neiman, and S. Kim, Phys. Rev. E **57**, 3292 (1998).

[6] S. R. Massanés and C. J. P. Vicente, Phys. Rev. E **59**, 4490 (1999).

[7] B. Lindner and L. Schimansky-Geier, Phys. Rev. E **60**, 7270 (1999).

[8] J. R. Pradines, G. V. Osipov, and J. J. Collins, Phys. Rev. E **60**, 6407 (1999).

[9] D. E. Postnov, S. K. Han, T. Y. Yim, and O. V. Sosnovtseva, Phys. Rev. E **59**, 3791 (1999).

[10] W. Ebeling, H. Herzel, W. Richert, and L. Schimansky-Geier, Z. Angew. Math. Mech. **66**, 141 (1986).

[11] Ch. Kurrer and K. Schulten, Phys. Rev. E **51**, 6213 (1995).

[12] L. Gammaitoni, P. Hänggi, P. Jung, and F. Marchesoni, Rev. Mod. Phys. **70**, 223 (1998); F. Moss, D. Pierson, and D. O. O'Gorman, Int. J. Bifurcation Chaos Appl. Sci. Eng. **4**, 1383 (1994).

[13] J. J. Collins, C. C. Chow, and T. T. Imhoff, Phys. Rev. E **52**, 3321 (1995).

[14] D. R. Chialvo, A. Longtin, and J. Müller-Gerking, Phys. Rev. E **55**, 1798 (1997).

[15] A. Longtin, J. Stat. Phys. **70**, 309 (1993); Nuovo Cimento D **17**, 835 (1995).

[16] K. Wiesenfeld, D. Pierson, E. Pantazelou, C. Dames, and F.

Moss, Phys. Rev. Lett. **72**, 2125 (1994).

[17] X. Pei, K. Bachmann, and F. Moss, Phys. Lett. A **206**, 61 (1995).

[18] A. Longtin and D. R. Chialvo, Phys. Rev. Lett. **81**, 4012 (1998).

[19] D. Nozaki, D. J. Mar, P. Grigg, and J. J. Collins, Phys. Rev. Lett. **82**, 2402 (1999).

[20] A. R. Bulsara *et al.*, Phys. Rev. E **53**, 3958 (1996).

[21] T. Shimokawa, K. Pakdaman, and S. Sato, Phys. Rev. E **59**, 3427 (1999).

[22] T. Shimokawa, K. Pakdaman, and S. Sato, Phys. Rev. E **60**, R33 (1999).

[23] H. E. Plesser and T. Geisel, Phys. Rev. E **59**, 7008 (1999).

[24] R. A. FitzHugh, Biophys. J. **1**, 445 (1961); A. C. Scott, Rev. Mod. Phys. **47**, 487 (1975).

[25] J. D. Murray, *Mathematical Biology* (Springer, Berlin, 1993).

[26] S. Fauve and F. Heslot, Phys. Lett. **79A**, 5 (1983).

[27] B. McNamara and K. Wiesenfeld, Phys. Rev. A **39**, 4854 (1989).

[28] V. I. Melnikov, Phys. Rev. E **48**, 2481 (1993).

[29] P. Hänggi and H. Thomas, Phys. Rep. **88**, 207 (1982).

[30] F. Marchesoni, F. Apostolico, and S. Santucci, Phys. Rev. E **59**, 3958 (1999).

[31] R. L. Stratonovich, *Topics in the Theory of Random Noise* (Gordon and Breach, New York, 1967), Vol. 1.

[32] *Handbook of Mathematical Functions*, edited by M. Abramowitz and Irene A. Stegun (Dover, New York, 1970).

[33] J. J. Collins *et al.*, Nature (London) **376**, 236 (1995).

[34] A. R. Bulsara, S. B. Lowen, and C. D. Rees, Phys. Rev. E **49**, 4989 (1994).